IGARSS 2025 - 2025 IEEE International Geoscience and Remote Sensing Symposium | 979-8-3315-0810-4/25/$31.00 ©2025 IEEE | DOI: 10.1109/IGARSS55030.2025.11242886

IMAGING MODEL OF WIDEBAND VORTEX ELECTROMAGNETIC WAVES UNDER DISPERSION EFFECT

Yixin Wei[1,2,3], *Gaofeng Shu*[1,2,3,*], *Ning Li*[1,2,3]

[1]*School of Computer and Information Engineering, Henan University*
[2]*Henan Key Laboratory of Big Data Analysis and Processing, Henan University*
[3]*Henan Province Engineering Research Center of Spatial Information Processing, Henan University*
Kaifeng, 475004, China

ABSTRACT

The phase characteristics of vortex electromagnetic waves offer significant potential for forward-looking radar imaging. Previous vortex electromagnetic wave imaging systems often used narrowband linear frequency modulation (LFM) signals to obtain range information. However, to achieve a higher range resolution, it is necessary to increase the signal bandwidth. A commonly used method for generating vortex electromagnetic waves is utilizing a uniform circular array (UCA), where each array element requires a phase shifter to apply phase shifts, producing vortex electromagnetic waves of different modes. Due to the dispersion effect, for wideband signals, the phases generated by different antenna elements at various instantaneous frequencies do not conform to the specific phase pattern required for a particular vortex electromagnetic wave mode. This discrepancy causes the traditional imaging model to be unable to accurately describe the imaging process of wideband vortex electromagnetic waves. To address this issue, this paper first derives the electromagnetic antenna pattern of wideband vortex electromagnetic waves and, based on this model, establishes a forward-imaging echo model. Finally, the proposed forward-imaging model for wideband vortex electromagnetic wave radar is validated using the least squares method.

Index Terms— Orbital angular momentum (OAM), forward-looking imaging, dispersion effect

1. INTRODUCTION

Forward-looking radar imaging has significant application value in autonomous aircraft landing, terrain avoidance, and missile guidance [1]-[4]. In recent years, vortex electromagnetic waves carrying orbital angular momentum (OAM) have attracted widespread attention in forward-looking radar imaging due to their phase characteristics, which provide new degrees of freedom for signal processing [5]-[9]. There has been considerable research on vortex electromagnetic wave forward-looking radar imaging. For example, Qu et al. proposed an imaging algorithm based on low-rank and sparse joint constraints, and completed simulation experiments with a bandwidth of 200 MHZ, eliminating the influence of Bessel functions [10]. Wang et al. introduced a target 3D focusing imaging method based on back-projection (BP) and spectral estimation, verifying the effectiveness of their method with a bandwidth of 600 MHz [11]. Zhang et al. proposed an iterative adaptive super-resolution vortex radar imaging algorithm, which was validated with a bandwidth of 100 MHz [12]. Most of the existing studies on vortex electromagnetic wave radar imaging have been conducted under narrow bandwidth conditions, which limits the improvement of range resolution in 2D imaging.

Previous studies have mostly used uniform circular array (UCA) and phased array (PA) technology to generate vortex electromagnetic waves [13]-[15]. In these systems, each array element is equipped with a phase shifter to introduce incremental phase differences between adjacent channels. Under narrowband conditions, dispersion effect has little impact on vortex electromagnetic wave imaging. To improve range resolution, when wideband signals are used to generate vortex electromagnetic waves, we similarly aim to ensure that the wideband signal experiences the same phase delay through the phase shifters in order to maintain the ideal wavefront structure of the vortex electromagnetic waves. However, practical phase shifters cannot achieve this [17]. For wideband signals, significant dispersion effect lead to antenna pattern distorted such as main lobe broadening, side lobe elevation, and even lobe splitting, which cause a dramatic degradation in imaging quality.

In this paper, we first derive the electromagnetic field model of a UCA under the dispersion effect of phase modulation using wideband linear frequency modulation (LFM) signals and analyze the antenna pattern characteristics of vortex electromagnetic waves under dispersion effect. Subsequently, a theoretical wideband forward-imaging echo model is established under the influence of dispersion effect. Finally, the validity of the proposed imaging model is verified

This work was supported by the Natural Science Foundation of Henan under Grant 242300421170.
*Corresponding author: *Gaofeng Shu* (gaofeng.shu@henu.edu.cn).

using the least squares method.

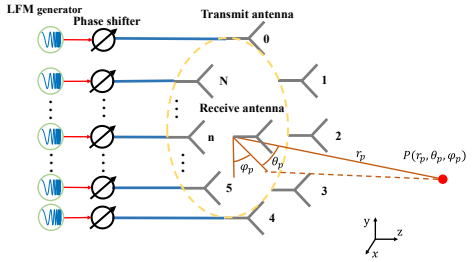

Fig. 1. Antenna array configuration.

2. WIDEBAND VORTEX ELECTROMAGNETIC WAVE ANTENNA PATTERN

Vortex electromagnetic waves can be generated through various combinations of excitation sources, and in this paper, a UCA is used. Fig. 1 shows the configuration of the UCA, where N transmitting antennas are evenly distributed along a circle with radius a. The phase difference between adjacent elements is $\varphi_n = 2\pi l(n-1)/N$, $n = 1,2,\dots,N$, where l represents the OAM mode number. The receiving antenna is placed at the center of the circle. Assuming that the elements of the UCA are dipole antennas, under a single-frequency condition, the electric field intensity $E(r)$ at any points in space can be expressed as [7]

$$E(r) = -j\frac{\mu_0 \omega d}{4\pi}\sum_{n=1}^{N}\frac{e^{-ik|r-r_n'|}}{|r-r_n'|}e^{il\varphi_n} \tag{1}$$

where j is the current density of the dipole antenna, and d is the length of the electric dipole. μ_0 is the permeability of free space, and ω and k are the angular frequency and wave number of the monochromatic signal, respectively, where $k = \frac{2\pi}{\lambda}$, with λ being the wavelength. The wavelength is related to the frequency by $\lambda = \frac{c}{f_c}$, where c is the speed of light and f_c is the signal frequency.

Using the infinitesimal dipole approximation, the magnitude $|r - r_n'|$ is approximated as r, and the phase approximation is given by $|r - r_n'| \approx r - a\sin\theta\cos(\varphi - \varphi_n)$. Thus, the above expression can be written as

$$E(r) = -j\frac{\mu_0 \omega}{4\pi}\frac{e^{ikr}}{r}\sum_{n=1}^{N}e^{i(ka\sin\theta\cos(\varphi-\varphi_n)+l\varphi_n)} \tag{2}$$

As N approaches infinity, according to the definition of the Bessel function, (2) can be written as

$$E(r) = -j\frac{\mu_0 \omega}{4\pi}\frac{e^{ikr}}{r}J_l(ka\sin\theta)e^{il\varphi} \tag{3}$$

where $J_l(x)$ represents the l-th order first kind Bessel function.

The above derivation shows the electric field expression of vortex electromagnetic waves generated by phase modulation of a monochromatic signal. However, for vortex electromagnetic waves imaging, high-range resolution information relies on transmitting wideband signals. The phase shifters connected with UCA elements used to generate vortex electromagnetic waves are not ideal, and the phase shifts applied to different frequency components are not completely consistent, thus introducing significant dispersion effect.

In order to obtain an ideal wideband vortex electromagnetic wave or a vortex electromagnetic wave with high mode purity, the phase shift of each frequency point of the signal should satisfy

$$\varphi_n = \frac{2\pi(n-1)}{N} = 2\pi f\Delta t(f) \tag{4}$$

where $\Delta t(f)$ is the delay introduced by phase shifter on a signal with frequency f.

Phase shifting a signal is equivalent to delaying it according to the signal's frequency. Therefore, when phase-shifting other frequency points based on the delay for the center frequency, the phase shift φ_n' is not equal to φ_n. φ_n' is expressed as

$$\varphi_n' = 2\pi f\Delta t(f_c) \tag{5}$$

where f is any frequency of the generated LFM signal, and f can be expressed as

$$f = f_c + K_r t \tag{6}$$

where K_r is the chirp rate, and t represents the fast time. Therefore, φ_n' can also be expressed as

$$\varphi_n' = 2\pi(f_c + K_r t)\Delta t(f_c) \tag{7}$$

Based on the above phase and electric field derivation process, substituting (7) into (2), the antenna pattern of wideband vortex electromagnetic waves in free space can be expressed as, and $E'(r)$ can be expressed as

$$E'(r) = -j\frac{\mu_0 \omega}{4\pi}\frac{e^{ik(f)r}}{r}\int e^{i(k(f)a\sin\theta\cos(\varphi-\varphi_n)+l\varphi_n')}dn \tag{8}$$

where $k(f)$ is a function of the wave number.

Due to the inconsistency in the signal frequencies, resulting in inconsistent phase modulation of the signal, it is necessary to perform a transformation on it

$$\varphi_n' = \frac{f}{f_c}\varphi_n \tag{9}$$

Then, the mode l is transformed as follows

$$l(f) = \frac{f}{f_c}l \tag{10}$$

As can be seen from the above expression, the dispersion effect also affects the generated vortex electromagnetic wave modes.

Substituting the above expression into (9), we obtain

$$\begin{aligned} E'(r) &= -j\frac{\mu_0 \omega}{4\pi}\frac{e^{ik(f)r}}{r} \\ &\int e^{ik(f)a\sin\theta\cos(\varphi-\varphi_n)}e^{il(f)\varphi_n}dn \\ &= -j\frac{\mu_0 \omega}{4\pi}\frac{e^{ik(f)r}}{r}J_{l(f)}[k(f)a\sin\theta]e^{jl(f)\varphi} \end{aligned} \tag{11}$$

For the convenience of establishing the subsequent imaging model, based on the time-frequency relationship of the LFM signal, $E'(r)$ can be written as

$$E'(r) = -j\frac{\mu_0 \omega}{4\pi}\frac{e^{ik(t)r}}{r}J_{l(t)}[k(t)a\sin\theta]e^{jl(t)\varphi} \tag{12}$$

Based on the derived antenna pattern results, it is evident

that when wideband LFM signals are modulated using a UCA, the generated pattern results in free space exhibits frequency-dependent characteristics due to dispersion effect. When utilizing wideband LFM signals to generate vortex electromagnetic waves, it becomes necessary to establish a new imaging model to mitigate the effect of dispersion. The process of developing this model is detailed in Section 3.

3. ECHO MODEL AND IMAGING METHOD

In the previous section, we derived the dispersion effect of vortex electromagnetic waves based on phase-modulated LFM signals. From Section 2, it can be inferred that dispersion effect leads to distortion of the antenna radiation pattern, which in turn causes the super-resolution imaging model to fail. In this section, we establish an imaging model for vortex electromagnetic waves under dispersion effect in wideband conditions and solve the model using the least squares method.

The imaging area is divided into q rows and m columns, with the total number of pixels equal to $q \cdot m$, where q is the number of sampling points in the range direction and m is the number of sampling points in the azimuth direction. A wideband LFM signal with phase modulation is transmitted using the UCA shown in Fig. 1, and single-antenna reception is used. Ignoring the constant term in (12), when the vortex electromagnetic waves illuminate the target $P(r_p, \theta_p, \varphi_p)$, the echo signal received by the antenna can be expressed as

$$S_r(l,t) = \sigma_p J_{l(t)}\left[k(t)asin\theta_p\right]e^{jl(t)\varphi_p} \mathrm{e}^{i2\pi fc(t-\frac{2r_p}{c})} e^{i\pi K_r\left(t-\frac{2r_p}{c}\right)^2} \tag{13}$$

Where σ_p is the backscatter coefficient at the target P.

To achieve high-range resolution, pulse compression must be performed on the echo. Therefore, the echo after down conversion and pulse compression can be expressed as

$$S_{rc}(l,t) = J_{l(t)}[k(t)asin\theta_i]e^{il(t)\varphi_p} \operatorname{sinc}\left[\mathrm{B_w}\left(\mathrm{t}-\frac{2\mathrm{r_p}}{c}\right)\right] e^{-j4\pi f_c\frac{r_p}{\lambda}} \tag{14}$$

Discretizing (14), the imaging area is illuminated by sequentially transmitting vortex electromagnetic waves with different OAM modes in a pulse-by-pulse manner, and the OAM modes spaced by 1, the above expression can be written as

$$S_{rc} = H\sigma + n \tag{15}$$

where n represents the additive noise, H is the observation matrix of the generated vortex electromagnetic wave in free space, and σ is the backscattering coefficient of the equivalent scattering center of the discretized grid in the imaging area. H and σ can be expressed as

$$H = \begin{bmatrix} h_{l_1}(t_1,\varphi_1) & h_1(t_1,\varphi_2) & \cdots & h_1(t_{T_p},\varphi_m) \\ h_{l_2}(t_1,\varphi_1) & h_2(t_1,\varphi_2) & \cdots & h_2(t_{T_p},\varphi_m) \\ \vdots & \vdots & \ddots & \vdots \\ h_{l_K}(t_1,\varphi_1) & h_L(t_1,\varphi_2) & \cdots & h_L(t_{T_P},\varphi_m) \end{bmatrix} \tag{16}$$

$$\sigma = [\sigma_{11} \quad \cdots \quad \sigma_{1m} \quad \sigma_{21} \quad \cdots \quad \cdots \quad \sigma_{qm}]^T \tag{17}$$

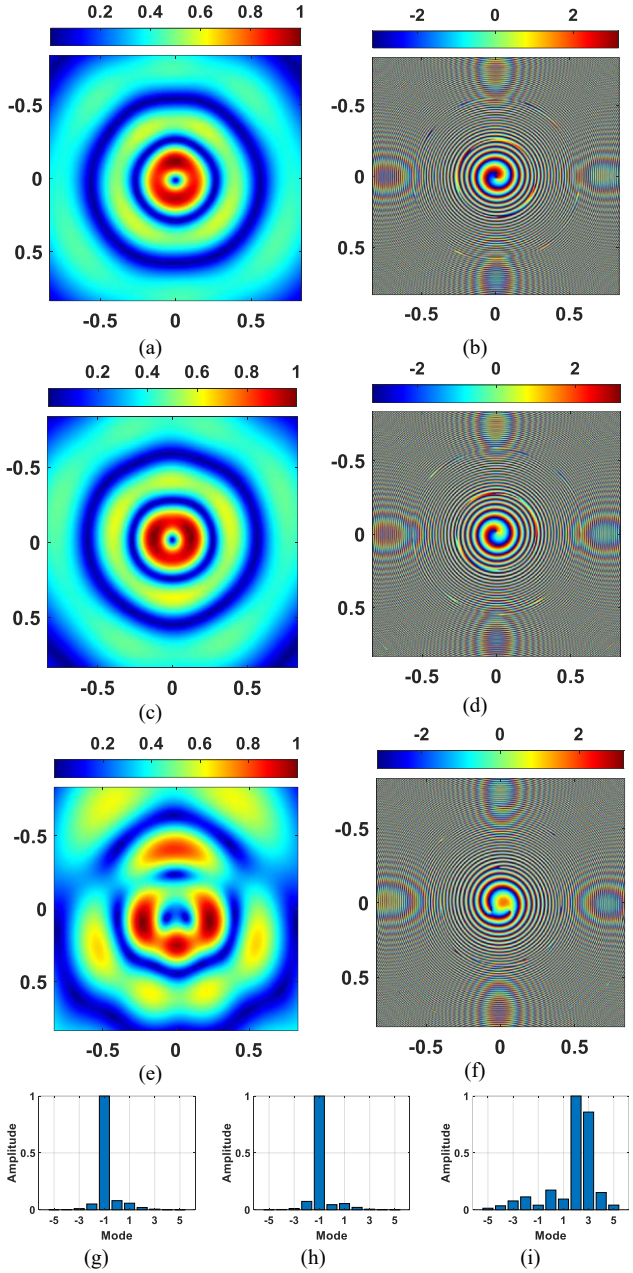

Fig.2. (a) and (c) are the near-field amplitude diagrams with instantaneous frequencies of 32 GHz and 40 GHz and mode -1, respectively. (e) is the near-field amplitude diagram with instantaneous frequency of 45 GHz and mode 2. (b) and (d) are the near-field phase diagrams with instantaneous frequencies of 32 GHz and 40 GHz and mode -1, respectively. (f) is the near-field phase diagram with instantaneous frequency of 45 GHz and mode 2. (g), (h) and (i) are the OAM spectra calculated from the main lobe of (a), (c) and (e).

where $h_{l_K}(t_n,\varphi_m)$ represents the electric field excitation formed at azimuth angle φ_m by the LFM signal at fast time t_n, l_K indicates the K-th mode of emission, and σ_{qm} represents the backscattering coefficient of the target in the q-th range cell and m-th azimuth cell, where $[\cdot]^T$ represents the transpose of the matrix.

$$h_{l(t_n)}(t_n,\varphi_m) = J_{l(t_n)}[k(t_n)asin\theta]e^{il(t_n)\varphi_m} \tag{18}$$

From (15), we can know, the imaging problem becomes a

problem of solving linear equation. Given the observation matrix H and the range-direction pulse-compressed matrix S_{rc}, the backscattering coefficient σ can be obtained by solving the following least-squares problem

$$\sigma = \arg\min_{\sigma} \left|\left|S_{rc} - H\sigma\right|\right|_2^2 \tag{19}$$

Since each imaging observation utilizes different OAM modes, which are mutually orthogonal, this ensures that the observation matrix H is full-rank. Consequently, it becomes feasible to independently extract information from different pixels, thereby enabling super-resolution imaging.

Differentiating (19) with respect to σ, and if $H^T H$ is nonsingular, then the unique solution for σ can be obtained as follows [13]

$$\sigma = [H^T H]^{-1} H^T S \tag{20}$$

By using the above equation, the focused 2D image can be obtained.

4. SIMULATION AND RESULTS

In this section, to analyze the impact of dispersion effect on the forward-looking radar imaging of vortex electromagnetic waves using wideband signals, we first simulated the antenna radiation patterns of vortex electromagnetic waves under different bandwidths. Fig. 3 shows the simulation results.

From Fig. 2(a) and (c), it can be observed that when the center frequency is 36 GHz and the instantaneous frequency of the LFM signal is 32 GHz and 40 GHz, the intensity patterns are distorted. From the phase patterns in Fig. 2(b) and (d), it can be seen that the phase still maintains a good linear relationship with the azimuth angle. However, by analyzing Fig. 2(g) and (h), it is found that due to the presence of dispersion effect, the generated vortex electromagnetic wave modes become impure. When the instantaneous frequency is 45 GHz, a noticeable effect is observed. The intensity pattern undergoes severe distortion, and within the main lobe, the phase pattern loses its linear variation characteristics. Fig. 2(i) shows a significant mode impurity phenomenon, all of which seriously affect the original imaging result.

Next, we set up a scenario with one point target, $P_1(550m, 0.25\pi, 0°)$ in the imaging scene and verify the proposed imaging model using the least squares method. The specific simulation parameters are shown in Table I.

TABLE I
SIMULATION PARAMETERS

Parameters	Value	Unit
Carry Frequency f_c	36	GHz
Bandwidth B_w	10	GHz
Mode Range l	-10:10	
Pulse width T_p	10	μs
Array radius a	2	λ

Fig. 3 shows the result obtained by solving the traditional imaging model using the least-squares method under the influence of dispersion effect [13]. From the result, we can see that normal focusing cannot be achieved due to the dispersion effect.

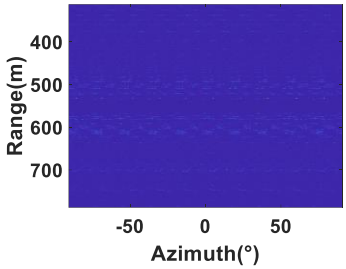

Fig. 3. The traditional model uses the least squares method to image the results.

Fig 4 (a) shows the focusing result obtained by FFT in the mode domain. It can be found that in the case of wideband signals, the existence of dispersion effect leads to increased side lobes and decreased resolution. Fig 4 (b) verifies this result.

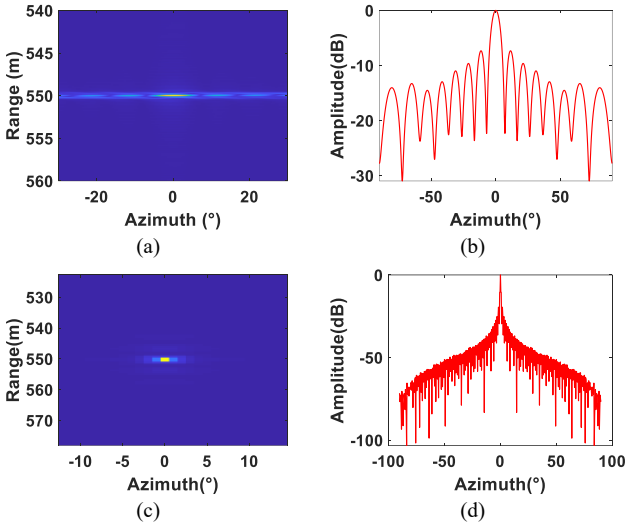

Fig.4. Imaging results. (a) FFT focusing results under the proposed model. (b) Azimuthal slice of (a). (c) Least squares method focusing results under the proposed model. (d) Azimuthal slice of (c).

By using the least squares method results obtained in Section 3, the imaging model proposed in this paper is solved to obtain the focusing result shown in Fig. 4 (c). It can be seen that the model proposed in this paper can still achieve good focusing under the influence of the dispersion effect of wideband signals. By comparing Fig. 4 (d) with Fig. 4 (b), we can easily see that under the imaging model of this paper, the azimuth resolution is not affected by the dispersion effect.

5. CONCLUSION

In this paper, a field model for generating vortex electromagnetic waves using phase-modulated LFM signals under wideband conditions is established. Based on this model, a new model for forward-looking radar imaging is constructed. Finally, the effectiveness of the proposed imaging model is validated through a least-squares method simulation experiment.

6. REFERENCES

[1] D. Schiavulli, F. Nunziata, G. Pugliano and M. Migliaccio, "Reconstruction of the Normalized Radar Cross Section Field From GNSS-R Delay-Doppler Map," *IEEE Journal of Selected Topics in Applied Earth Observations and Remote Sensing*, vol. 7, no. 5, pp. 1573-1583, May 2014.

[2] V. Malyavej, I. R. Manchester and A. V. Savkin, "Precision missile guidance using radar/video sensor fusion with a communication constraint," *2004 5th Asian Control Conference (IEEE Cat. No.04EX904)*, Melbourne, VIC, Australia, pp. 1817-1825 Vol.3, 2004.

[3] Y. Huang, Y. Zha, Y. Wang, and J. Yang, "Forward looking radar imaging by truncated singular value decomposition and its application for adverse weather aircraft landing," *Sensors*, vol. 15, no. 6, pp. 14 397–14 414,2015.

[4] X. Tuo, Y. Zhang, D. Mao, Y. Kang, and Y. Huang, "A radar forward-looking super-resolution method based on singular value weighted truncation," *IGARSS 2019-2019 IEEE International Geoscience and Remote Sensing Symposium*, pp. 9180–9183, 2019.

[5] B. Thidé, H. Then, and J. Sjöholm, "Utilization of photon orbital angular momentum in the low-frequency radio domain," *Phys.Rev.Lett*, vol. 99,no. 8, pp. 1–4, Aug. 2007.

[6] S. M. Mohammadi, L. K. S. Daldorff, and J. E. S. Bergman, "Orbital angular momentum in radio—A system study," *IEEE Trans. Antennas Propag*, vol. 58, no. 2, pp. 565–572, Feb. 2010.

[7] L. Allen, M. W. Beijersbergen, R. J. C. Spreeuw, and J. P. Woerdman,Orbital angular momentum of light and the transformation of laguerre-Gaussian laser modes," *Phys.Rev. A,Gen. Phys*, vol. 45, no. 11,pp. 8185–8189, Jun. 1992.

[8] A. M. Yao and M. J. Padgett, "Orbital angular momentum Origins,behavior and applications," *Adv. Opt. Photon*, vol. 3, no. 3, pp. 161–204,Jun. 2011.

[9] G. Shu et al., "A Novel Vortex Synthetic Aperture Radar Imaging System Decreasing the Pulse Repetition Frequency Without Increasing the Antenna Aperture," *IEEE Transactions on Geoscience and Remote Sensing*, vol. 60, pp. 1-14, 2022.

[10] H. Qu, S. Li, C. Chen, J. Liu and W. Chen, "High-Resolution Orbital Angular Momentum Imaging With the Removal of Bessel Function Modulation Effect," *IEEE Transactions on Microwave Theory and Techniques*, vol. 72, no. 4, pp. 2577-2590, April 2024.

[11] J. Wang, K. Liu, H. Liu, K. Cao, Y. Cheng and H. Wang, "3-D Object Imaging Method With Electromagnetic Vortex," *IEEE Transactions on Geoscience and Remote Sensing*, vol. 60, pp. 1-12, 2022, Art no. 2000512.

[12] X. Zhang, L. Wang, W. Li, Z. Li and J. Wu, "Vortex Radar Super-resolution Imaging Based on Iterative Adaptive Approach," *2021 CIE International Conference on Radar (Radar)*, Haikou, Hainan, China, pp. 824-827, 2021.

[13] T. Yuan, H. Liu, Y. Cheng, Y. Qin and H. Wang, "Orbital-angular-momentum-based electromagnetic vortex imaging by least-squares method," *2016 IEEE International Geoscience and Remote Sensing Symposium (IGARSS)*, *Beijing, China*, pp. 6645-6648, 2016.

[14] H. Zhao and K. Wang, "Orbital-Angular-Momentum-Based Radar Imaging By Dice Regularized Orthogonal Matching Pursuit," *2020 IEEE 5th International Conference on Signal and Image Processing (ICSIP)*, Nanjing, China, pp. 446-450, 2020.

[15] K Liu, H Liu, H Wang, X Li. "Vortex electromagnetic wave imaging with orbital angular momentum and waveform degrees of freedom". *Opt Express*, 32(8)13574-13582, Apr 2024.

[16] H. Qu, D. Cheng, C. Chen and W. Chen, "Sparsity-driven high-resolution fast electromagnetic vortex imaging based on two-dimensional NCALM," *2020 IEEE 6th International Conference on Computer and Communications (ICCC)*, Chengdu, China, pp. 1880-1885, 2020.

[17] J. Ma, J. Cai, Z. Zheng, X. Gao and S. Huang, "Spatiotemporal Evolution of Orbital Angular Momentum (OAM) Beams Based on a Uniform Circular Frequency Diverse Array (UC-FDA)," in *IEEE Transactions on Antennas and Propagation*, vol. 71, no. 5, pp. 4183-4193, May 2023.